Global distribution of groundwater-vegetation spatial covariation

Postprint version

Sujan Koirala, Martin Jung, Markus Reichstein, Inge E. M. de Graaf, Gustau Camps-Valls, Kazuhito Ichii, Dario Papale, Botond Ráduly, Christopher R. Schwalm, Gianluca Tramontana and Nuno Carvalhais

Published in: **Geophysical Research Letters**

Reference: Koirala, S., Jung, M., Reichstein, M., de Graaf, I. E. M., Camps-Valls, G., Ichii, K., et al. (2017). Global distribution of groundwater-vegetation spatial covariation. Geophysical Research Letters, 44(9), 4134-4142. doi:10.1002/2017GL072885

Web link: http://dx.doi.org/10.1002/2017GL072885

This project has received funding from the European Union's Horizon 2020 research and innovation programme under grant agreement No 640176

Geophysical Research Letters

RESEARCH LETTER
10.1002/2017GL072885

Key Points:
- Local-scale groundwater-vegetation spatial covariations are prevalent globally
- Both positive and negative relationships are equally widespread
- There is a stronger association of the sign of relationship with vegetation than with climate and land surface characteristics

Supporting Information:
- Supporting Information S1

Correspondence to:
S. Koirala,
skoirala@bgc-jena.mpg.de

Citation:
Koirala, S., et al. (2017), Global distribution of groundwater-vegetation spatial covariation, Geophys. Res. Lett., 44, 4134–4142, doi:10.1002/2017GL072885.

Global distribution of groundwater-vegetation spatial covariation

Sujan Koirala[1], Martin Jung[1], Markus Reichstein[1], Inge E. M. de Graaf[2,3], Gustau Camps-Valls[4], Kazuhito Ichii[5,6,7], Dario Papale[8,9], Botond Ráduly[8,10], Christopher R. Schwalm[11,12], Gianluca Tramontana[8], and Nuno Carvalhais[1,13]

[1]Department of Biogeochemical Integration, Max Planck Institute for Biogeochemistry, Jena, Thuringia, Germany, [2]Department of Physical Geography, Utrecht University, Utrecht, Netherlands, [3]Department of Geology and Geological Engineering, Colorado School of Mines, Golden, Colorado, USA, [4]Image Processing Laboratory, University of Valencia, Paterna, Valencia, Spain, [5]Department of Environmental Geochemical Cycle Research, Japan Agency for Marine-Earth Science and Technology, Yokohama, Kanagawa, Japan, [6]Center for Global Environmental Research, National Institute for Environmental Studies, Tsukuba, Ibaraki, Japan, [7]Center for Environmental Remote Sensing, Chiba University, Chiba, Japan, [8]Dipartimento per l'Innovazione nei Sistemi Biologici, Agroalimentari e Forestali, Università della Tuscia, Viterbo, Lazio, Italy, [9]Centro Euro-Mediterraneo sui Cambiamenti Climatici, Lecce, Apulia, Italy, [10]Department of Bioengineering, Sapientia Hungarian University of Transylvania, Miercurea Ciuc, Centru, Romania, [11]Woods Hole Research Center, Falmouth, Massachusetts, USA, [12]College of Engineering, Forestry, and Natural Sciences, Center for Ecosystem Science and Society, Northern Arizona University, Flagstaff, Arizona, USA, [13]CENSE, Departamento de Ciências e Engenharia do Ambiente, Faculdade de Ciências e Tecnologia, Universidade Nova de Lisboa, Almada, Lisbon, Portugal

Abstract Groundwater is an integral component of the water cycle, and it also influences the carbon cycle by supplying moisture to ecosystems. However, the extent and determinants of groundwater-vegetation interactions are poorly understood at the global scale. Using several high-resolution data products, we show that the spatial patterns of ecosystem gross primary productivity and groundwater table depth are correlated during at least one season in more than two thirds of the global vegetated area. Positive relationships, i.e., larger productivity under shallower groundwater table, predominate in moisture-limited dry to mesic conditions with herbaceous and shrub vegetation. Negative relationships, i.e., larger productivity under deeper groundwater, predominate in humid climates with forests, possibly indicating a drawdown of groundwater table due to substantial ecosystem water use. Interestingly, these opposite groundwater-vegetation interactions are primarily associated with differences in vegetation than with climate and surface characteristics. These findings put forth the first evidence, and a need for better representation, of extensive and non-negligible groundwater-vegetation interactions at the global scale.

1. Introduction

Groundwater is a critical source of soil moisture supply for evapotranspiration [Lautz, 2008; Martinet et al., 2009; Niu et al., 2007; Yeh and Famiglietti, 2009] and its components [Cramer et al., 1999; Maxwell and Condon, 2016] when radiation energy is abundant and precipitation is limited. Several studies have shown that under such moisture-limited conditions, this additional moisture supply also enables vegetation to limit the loss of productivity [Gou et al., 2015], especially in water-limited ecosystems [Baldocchi et al., 2010; Barbeta et al., 2015]. This access to and potential dependence on below-ground moisture supply from groundwater can even shape local-scale vegetation distribution and species segregation [Orellana et al., 2012; Silvertown et al., 2015], and it has been speculated that groundwater may also be a key driver of ecological patterns globally [Fan, 2015]. Unfortunately, efforts to link such patterns have been limited to the local scale in experimental studies and regional scale in remote-sensing or model-based studies (see Eamus et al. [2015] for an in-depth review). At the global scale, we still lack any knowledge on the relevance, extent, timing, and conditions leading to the groundwater-vegetation interactions.

The global-scale efforts to link groundwater and vegetation patterns have been impeded by a dearth of higher resolution data sets and models that consider both groundwater and vegetation processes [Bierkens et al., 2015]. As the collection of field observation data is impractical for regional- and global-scale studies, remote sensing data are suitable to identify groundwater-dependent ecosystems over a large spatial scale [Eamus et al., 2015; Pérez Hoyos et al., 2016]. The remote sensing data have successfully been used to link

terrestrial water storage variations (total storage including groundwater) and vegetation activities on a regional scale [A et al., 2015; McGrath et al., 2012; Yang et al., 2014]. Due to recent advances in Earth observation networks and modeling approaches, we can now investigate the relationship between fine-grained spatial patterns of groundwater and vegetation productivity in the global context as well.

In this study, we exploit relatively high spatial resolution (~10 km) global data sets of model-based groundwater table depth (WTD) together with gross primary productivity (GPP) derived from satellite remote sensing, FLUXNET observations, and multiple machine learning methods to identify where, when, and how spatial patterns of GPP and WTD are related globally. We then assess how these spatial patterns are associated with vegetation, land surface, and climate characteristics.

2. Data and Methods

The GPP data, at ~10 km spatial and 8 daily temporal resolution, were obtained from FLUXCOM [FLUXCOM, 2017; Jung et al., 2017; Tramontana et al., 2016]. Using nine machine learning algorithms, two observed GPP variants from two flux partitioning methods [Lasslop et al., 2010; Reichstein et al., 2005] were upscaled from 224 FLUXNET sites [Baldocchi et al., 2001] to the global scale. The machine learning algorithms were initially trained to site-level observations of the explanatory climate and land surface variables. To capture variabilities in vegetation greenness and land surface temperature with reliable imprint of changes associated with groundwater, the variables from high-resolution satellite remote sensing data were fed into the extensive variable selection analysis [Jung and Zscheischler, 2013]. The machine learning algorithms and their training and a thorough cross-validation of the data are presented in detail in Tramontana et al. [2016]. To obtain the global GPP, the trained and validated machine learning algorithms were forced with global gridded satellite data of selected explanatory variables, at 10 km spatial and 8 daily temporal resolution, to obtain the GPP for the period of 2001–2012. In total, 18 variants (two observed GPP variants and nine algorithms) of global GPP time series were produced, and the ensemble median was used in this study.

Compared to other global GPP products, the median GPP from FLUXCOM is advantageous because it combines the strengths of multiple global satellite-based observations with site-level observations using several methods. The GPPs estimated only by a subset of algorithms used in FLUXCOM have shown better performance than the GPP from Moderate Resolution Imaging Spectroradiometer (MODIS) against site-level observations [Ichii et al., 2017; Tramontana et al., 2015; Yang et al., 2007]. At the global scale, the Model Tree Ensembles GPP product [Beer et al., 2010; Jung et al., 2011], also estimated by a subset of algorithms used in FLUXCOM, compares well with modern satellite observation of Sun-induced fluorescence [Frankenberg et al., 2013], and it has been used extensively to benchmark global land surface models [Anav et al., 2013; Bonan et al., 2012; Piao et al., 2013].

The WTD data were obtained from an observation-constrained global-scale groundwater model simulation that considers the lateral groundwater flow [de Graaf et al., 2015]. Mean seasonal climatology of WTD is available at ~10 km spatial and monthly temporal resolutions. Forced by climate-driven recharge, land surface, and aquifer parameters, their groundwater model distributes the groundwater recharge laterally based on topography with coasts and river channels as boundary conditions. The WTD simulation was validated against >1.6 million site-level WTD observations. See section S1 in the supporting information for details.

To characterize the spatial covariation of GPP and WTD, we calculated Spearman's rank correlation coefficient within 11,134 river basins [Lehner et al., 2008] smaller than ~100,000 km^2 globally (see section S2). For a given basin, the correlation coefficient was calculated between two (or more for partial correlation coefficient) vectors of data variables from all the 10 km grid cells within the basin boundary. The Spearman's correlation is suitable here because it quantifies the covariation of spatial patterns which, for WTD, are well constrained by topography and bedrock information and, for GPP, by remote sensing of land surface characteristics. We test the statistical significance of the correlation at 5% level of significance.

These GPP-WTD Spearman's correlations were then controlled for five confounding climatic and land surface variables: precipitation, net radiation, topography/elevation, porosity, and leaf area index to eliminate the "background" collinearity. Precipitation and net radiation represent the moisture and energy available, respectively. Topography drives the spatial variation of WTD, and shallower WTDs usually occur at lower elevation. In addition, elevation differences also account for variation in temperature, which in turn relates

Table 1. A Summary of Data Sets Used in This Study

Variable	Temporal Resolution	Temporal Period	Spatial Resolution (km)	Spatial Domain	Source
GPP	8 daily	2001–2012	10	Global	Satellite/machine learning [FLUXCOM, 2017; Jung et al., 2017; Tramontana et al., 2016]
WTD	Monthly	Climatology	10	Global	Model-based [de Graaf et al., 2015]
Net radiation	8 daily	2001–2012	10	Global	Satellite/machine learning [FLUXCOM, 2017; Jung et al., 2017; Tramontana et al., 2016]
Precipitation	30 min	1998–2013	8	60°S-60°N	Multiple satellites [Joyce et al., 2004; NOAA, 2011]
Elevation	Static		1	Global	Satellite/cartography [USGS, 1996]
Soil porosity	Static		1	Global	Statistical/various [Dirmeyer et al., 2006; Hamonized World Soil Database, 2008]
Leaf area index	8 daily	2001–2012	10	Global	Satellite [Moderate Resolution Imaging Spectroradiometer, 2012]
Climate class	Static		50	Global	Climate data [Kottek et al., 2006]
Vegetation class	Static		1	Global	Satellite [Moderate Resolution Imaging Spectroradiometer, 2012]
Tree cover	Static		10	Global	Satellite [Defries et al., 2000]
Grass cover	Static		1	Global	Satellite [Jung et al., 2006]
C4 cover	Static		1	Global	Satellite [Jung et al., 2006]

to vapor pressure deficit, a driver of transpiration and GPP. Soil porosity, the potential soil moisture content, affects groundwater recharge and resistance against evapotranspiration. Finally, leaf area index (LAI) accounts for differences in vegetation types within a basin. The data sets of these variables were obtained from several observation-based or model-based sources. A summary of these data is provided in Table 1, and they are explained in detail in section S1. As these data are either based on high-resolution satellite or topographic data, we assume that they represent the spatial variability well. The assumption is a necessity, as there are no global modeling or observation frameworks that could produce all the data needed in a consistent manner.

Since the GPP are positive and WTD are negative numbers while calculating (partial) correlation coefficient, the GPP-WTD correlation is positive for a basin when the grids with larger GPP have shallower WTD (smaller magnitude of a negative number). In contrast, a negative GPP-WTD correlation indicates that grids with larger GPP have deeper WTD. For each basin, the GPP-WTD correlation was calculated seasonally for four phenological stages of the vegetation derived from GPP (see sections S3 and S4 and Forkel et al. [2014]). The correlation coefficient over four seasons is then used to identify the dominant sign of GPP-WTD spatial correlation. The dominant GPP-WTD correlation for a basin is defined as the sign, positive or negative, of the correlation that dominates over four phenological stages. To identify the dominant correlation, we first record the sign of a significant correlation ($p < 0.05$) in each phenological stage, and then calculate the difference in number of seasons with positive correlation minus that with negative correlation. This generalization using the dominant GPP-WTD correlation is reasonable because the sign of GPP-WTD correlation does not change in different phenological stages for 89% of the basins (see section S5 for a detailed explanation). The main text here focuses on the dominant GPP-WTD correlation, while a complete analysis for each phenological stage is presented in the supporting information.

3. Results and Discussions

We first present the results for global distribution of the dominant GPP-WTD correlation. Then, we investigate the association of the dominant correlation with vegetation, surface, and climate characteristics. Finally, we evaluate the relative importance of vegetation, surface, and climate characteristics in determining the sign of the dominant GPP-WTD correlation.

3.1. Global Distribution of GPP-WTD Correlation

The GPP-WTD correlations are statistically significant in at least one season for roughly two thirds of the vegetated area (Figure 1). Temporally, the correlation is statistically significant in only one season for 21% and in two seasons for further 15% of the basins. This shows that the groundwater-vegetation interaction,

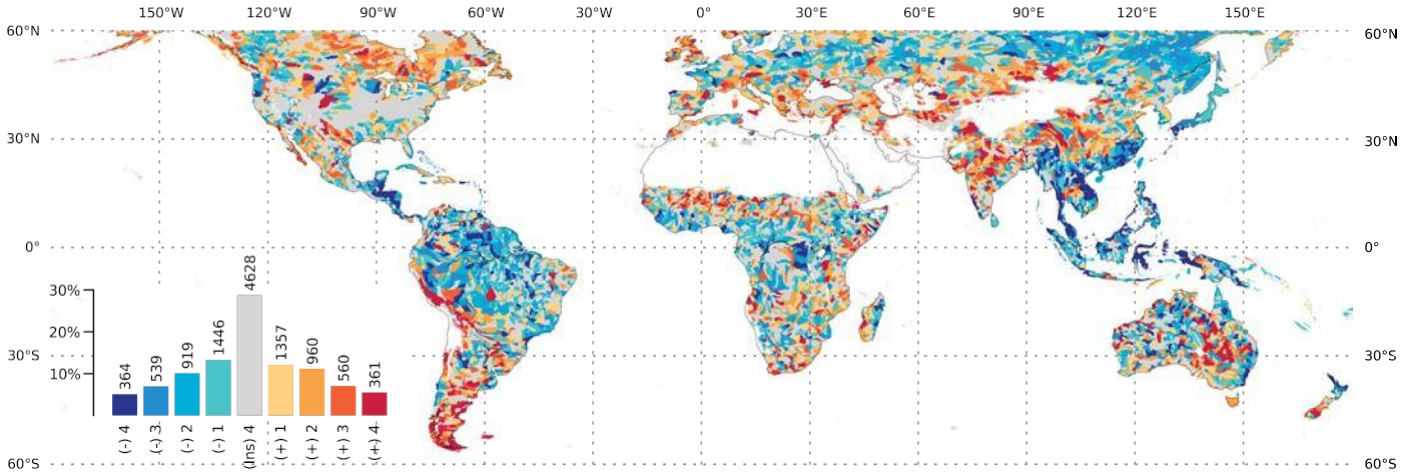

Figure 1. Global distribution of the dominant GPP-WTD relationship. The red (blue) shades are used for basins where the number of seasons with positive correlation is larger (smaller) than that with negative correlation. The basins in which GPP-WTD correlation is statistically insignificant in all seasons are shaded grey. In the bar chart, the height of a bar shows the areal coverage (relative to total global vegetated area), while the number above each bar is the number of basins.

either positive or negative, is significant under certain "ecohydrologically relevant" condition only and has strong temporal dynamics. Further, the areal extent of significant positive correlation is the largest when GPP is minimum, showing that positive correlation predominates when vegetation activity is limited. In contrast, the negative correlation predominates when vegetation activity is maximum (see section S5 for details).

Even though the basins dominated by positive and negative GPP-WTD correlations have similar areal extents globally, they have a distinct spatial footprint. The positive relationship prevails in ~36% of the vegetated area, located primarily in the Indian subcontinent, sub-Saharan Sahel regions, semiarid regions of eastern and southern Africa, noncoastal regions of southern and eastern Australia (in and around Lake Eyre basin), Eurasian midlatitudes, and northern parts of North America. In most of these regions with typically limited moisture supply, groundwater is likely supporting primary productivity through enhanced soil moisture availability. This is also consistent with earlier model-based findings of sizable groundwater-supplied evapotranspiration in the semiarid regions globally [Koirala et al., 2014] as well as those in seasonally dry northern high-latitude regions [Cohen et al., 2006] and regions with higher probability of using nonprecipitation moisture sources in Australia [Doody et al., 2017].

A negative GPP-WTD relationship predominates in ~36% of the global vegetated area, and it is mostly evident in humid regions concentrated in tropical regions of South America, Africa, Southeast Asia, and parts of northern and northeastern Eurasia. Such an extensive negative GPP-WTD relationship was unexpected, as the previous studies signify, almost exclusively, the positive effect of groundwater on productivity. However, a negative GPP-WTD relationship might emerge due to several mechanisms such as suppression of GPP via anaerobic stress under very shallow WTD [Naumburg et al., 2005] or via a loss of leaves [Parolin and Wittmann, 2010] and structural disturbances [Moreno-Casasola and Vázquez, 1999] in floodplains. Furthermore, and perhaps more essentially and widespread, the WTD may become deeper with increasing GPP through simultaneously increasing evapotranspiration [Jung et al., 2011] and decreasing groundwater recharge.

Nearly 30% of the total vegetated area shows no significant GPP-WTD correlation in any season. There is no spatial coherency of insignificant relationship apart from an extensive area within the contiguous U.S., which might be related to large-scale anthropogenic irrigation that also affects GPP-WTD relationship [Kath et al., 2014]. Uncertainties of the WTD and GPP products likely weaken correlation coefficients as well. We carried out an additional analysis using an independent WTD data from Fan et al. [2013] (section S7). Despite a significant difference in the magnitude of WTD in two data products, the analysis reveals consistent spatial patterns of positive and negative GPP-WTD relationships globally. This is due to a similar regional spatial variability of two data, as WTD is mainly driven by topography in both cases.

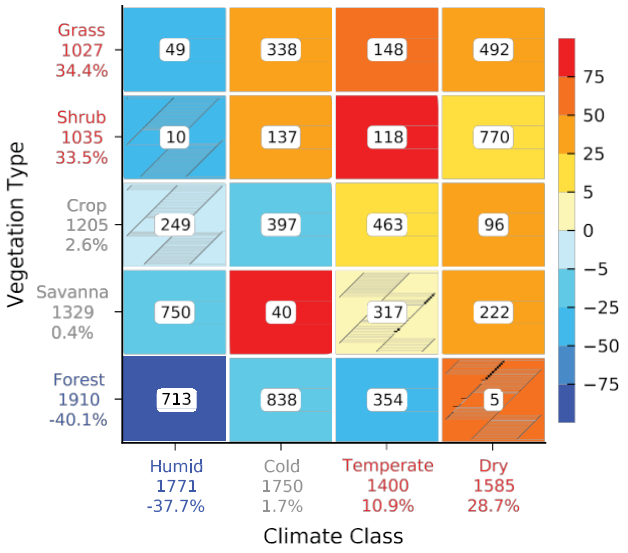

Figure 2. Distribution of basins dominated by positive and negative GPP-WTD relationships against simplified climate class and vegetation types. For each simplified climate class (from Köppen-Geiger climate classification) and vegetation type (from MODIS plant functional type), the total number of basins (inset number) is divided into those dominated by positive and negative GPP-WTD relationship, and the relative difference (in percentage) between the two is plotted. For the hatched blocks (insignificant difference), the relative difference is smaller than that caused by random effects. A summary for each climate class and vegetation type is provided in the axis labels. The ones dominated by positive (negative) relationship are colored red (blue), and the insignificant ones are colored grey.

3.2. Association With Vegetation, Surface, and Climate Characteristics

To characterize the determinants of the dominant GPP-WTD correlation, we segregated the occurrences of dominant positive and negative relationships for different climate and vegetation classes. We find that negative relationships prevail in humid climate and positive relationships prevail in dry climate irrespective of the vegetation types (Figure 2). In transient climates that are neither strictly humid nor dry, there is a substantial heterogeneity with respect to different vegetation types. In these temperate and seasonally cold regions, there is a clear distinction between prevailing negative relationships for forests and prevailing positive relationships for shrub or grasslands. For Savannas, mixed tree-grass systems, and crops (which are highly managed), there is no clear pattern on whether positive or negative GPP-WTD relationships dominate.

To further identify possible driving mechanisms behind variability of GPP-WTD relationship, we dissected the occurrences of positive and negative relationships against gradients of vegetation characteristics (leaf area index, fractions of tree [Defries et al., 2000] and grass covers, relative fraction of vegetation with C4 photosynthesis [Jung et al., 2006]), and the most important climatic variables (precipitation and net radiation). Because the mean WTD and GPP are independent of the spatial GPP-WTD correlation, they were also included in the analysis.

In general, the dominant sign of GPP-WTD relationships relates more strongly to differences in vegetation characteristics than to differences in mean climate characteristics (Figure 3). The Kolmogorov-Smirnov two-sample test (see section S9 for details) also reveals that the differences in the distribution of the occurrences of positive and negative GPP-WTD relationships are statistically significant ($p < 0.05$) against the proxies of vegetation structure and productivity (except relative fraction of C4 vegetation). While the number of basins with positive GPP-WTD relationships decreases with increasing GPP, LAI, and tree cover (Figures 3a–3c), it increases with increasing grass cover and relative fraction of vegetation with C4 photosynthesis (Figures 3d and 3e).

The stronger association of vegetation characteristics with the difference in the sign of GPP-WTD relationship might result from different connections between WTD, root depth [Fan, 2015; Tron et al., 2014], and distribution [Grimaldi et al., 2015], as well as from plant physiological factors affecting water use [Rodriguez-Iturbe et al., 2007]. For example, deeper tree roots (compared to those of shrub or grass) provide access to a

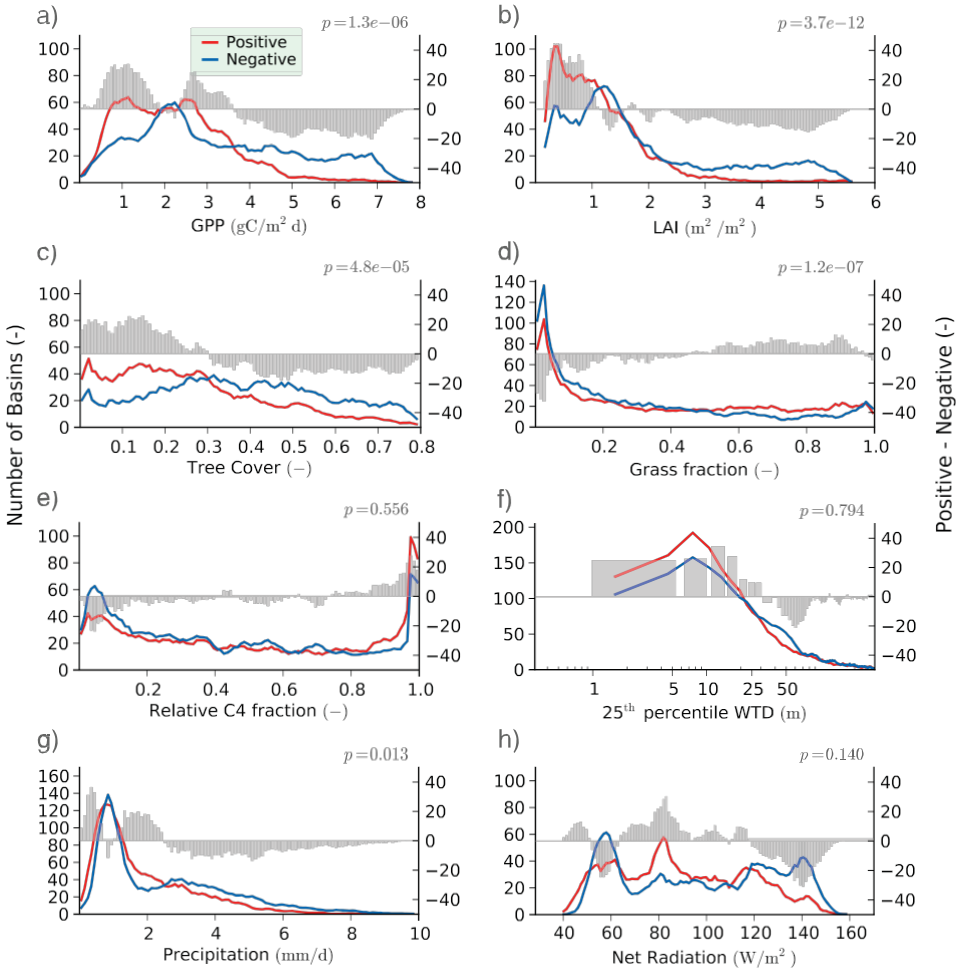

Figure 3. Distribution of vegetation, surface, and climate characteristics in basins dominated by positive and negative GPP-WTD relationship. In the left axis, the number of basins (red line for positive and blue line for negative) is plotted against (a) GPP, (b) leaf area index, (c) tree cover fraction, (d) grass cover fraction, (e) relative fraction of C4 vegetation, (f) 25th percentile WTD, (g) mean annual precipitation, and (h) net radiation. In the right axis, the difference in number of basins (positive minus negative) is plotted (grey bars). The P values of the Kolmogorov-Smirnov test of significance between the distributions of positive and negative relationships are provided on the top-right section of each plot. Note the irregular vertical axis limits, as well as the logarithmic horizontal axis in Figure 3f.

deeper soil column [Neill et al., 2013] under both normal and dry conditions [Baldocchi et al., 2004; Weltzin and McPherson, 1997], which increases the potential water uptake. This large water uptake decreases soil moisture and, consequently, groundwater recharge and results in a deeper WTD leading to a negative GPP-WTD relationship. On the other hand, the enhanced water use efficiency of vegetation with C4 photosynthesis [Still et al., 2003] facilitates a higher productivity per additional unit of soil moisture supply from groundwater, which could explain the prevalence of positive GPP-WTD relationship at the highest relative fraction of C4 vegetation (>90%).

The number of both positive and negative GPP-WTD relationships peaks at relatively low precipitation (300–400 mm/yr; Figure 3g) and shallow WTD (<10 m; Figure 3f), while no clear pattern is evident for net radiation (Figure 3h). We observe a statistically significant pattern ($p < 0.05$) of more negative GPP-WTD relationships with increasing precipitation (Figure 3g), suggesting that WTD deepens due to a large productivity and transpiration loss when the moisture supply from rainfall is abundant. Positive relationships prevail at shallow WTD (6–8 m), where groundwater capillary flux can be expected to enhance root zone moisture and surface water fluxes [Koirala et al., 2014]. Such shallow WTD conditions are particularly necessary for grass and shrub vegetation with shallower roots and limited direct access to groundwater.

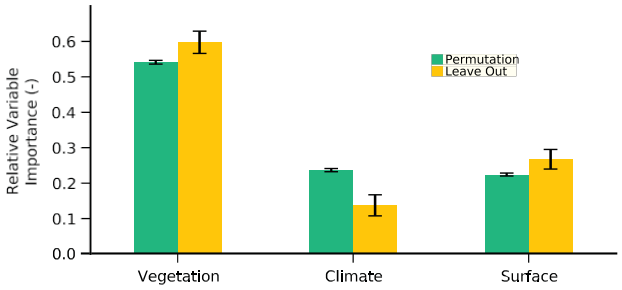

Figure 4. Relative importance of vegetation, climate, and surface characteristics in determining the dominant sign of GPP-WTD relationship. The vegetation characteristics include simplified MODIS vegetation type, GPP, leaf area index, tree cover, grass cover, relative fraction of C4 vegetation, and the phenological stage. The climate characteristics include precipitation, net radiation, and Köppen-Geiger climate class. The surface characteristics include WTD, elevation, and soil porosity. The relative importance is computed using two approaches, permutation and leave out (see section S10), which are each run 1000 times. The mean from 1000 runs is plotted as bars, and the values within ±1 standard deviation are plotted as error bars.

3.3. Relative Importance of Vegetation, Surface, and Climate Characteristics

Finally, we quantify the relative importance of climate (three variables), vegetation (seven variables), and surface (three variables) characteristics for the dominant sign of GPP-WTD correlation. To do so, we first trained a random forest classification algorithm [Breiman, 2001] to predict whether the GPP-WTD correlation is dominated by a positive or negative relationship. The relative importance of the groups of variables was then calculated using two methods; permutation and leave out approaches (see section S10). Irrespective of the metric chosen, vegetation-related predictors have a much larger relative importance than climate and land surface-related predictors in determining the dominant GPP-WTD correlation (Figure 4), which is also evident at the seasonal scale (Figures S13 and S14 in the supporting information). An additional calculation using only two principal components of each group of variables also produces a similar result (Figure S15), showing that the collinearity and difference in the number of variables within each group have little effect on relative importance.

4. Conclusions

This analysis has uncovered patterns of complex but spatially coherent and statistically significant distribution of positive or negative groundwater-vegetation relationships during at least one season in ~72% of the global vegetated land surface. This clearly demonstrates a global relevance of, often excluded, groundwater-vegetation interactions.

Whether groundwater may be supporting vegetation (yielding a positive relationship) or vegetation may be affecting groundwater (yielding a negative relationship) relates with climate, and more importantly, with characteristics of the vegetation itself. Because causality cannot be inferred from correlation coefficients alone, appropriate ecosystem model developments are urgently needed to quantify the groundwater-vegetation interactions at the global scale. It is especially critical because both positive and negative relationships are equally extensive at the current state, but their patterns and extents can be altered due to global climate and land cover changes. It implies that the recent trends and future projections of declining groundwater resources [Richey et al., 2015] and forest cover [Hansen et al., 2013], along with an increasing vegetation water use efficiency due to CO_2 fertilization [Keenan et al., 2013], would potentially shift the groundwater-vegetation interactions. The understanding of how groundwater-vegetation interactions respond to changes in climate and anthropogenic influence is crucial to quantify ecosystem services of groundwater and vegetation resources.

Acknowledgments

S.K. was financially supported by the ClimAfrica and EMBRACE (283201) projects of the European Commission under the 7th Framework Programme (FP7). M.J. and M.R. acknowledge the support of BACI project funded by the European Union's Horizon 2020 Research and Innovation program under grant agreement 640176. I.D.G. was supported by the Netherlands Organization for Scientific Research (NWO) under the program "Planetary boundaries of the global freshwater cycle." G.C.-V. was supported by the EU under the European Research Council (ERC) consolidator grant SEDAL-647423. K.I. was supported by the JSPS KAKENHI (25281003) and the Environment Research and Technology Development Funds (2-1401) from the Ministry of the Environment of Japan. C.R.S. was also supported by the National Aeronautics and Space Administration (NASA) grants NNX12AK12G, NNX12AP74G, NNX10AG01A, and NNX11AO08A. N.C. acknowledges the support of NOVA grant UID/AMB/04085/2013. The data for mean seasonal cycles of gross primary productivity and net radiation from FLUXCOM (http://www.fluxcom.org) and water table depth are available from the data portal of Max Planck Institute for Biogeochemistry (https://www.bgc-jena.mpg.de/geodb/FluxCom/gw-veg.php) after registration. For convenience, the sources of other publicly available data sets used in this study are also consolidated in the above webpage. We express our gratitude to Fabian Gans and Gerhard Boenisch at Max Planck Institute for Biogeochemistry for setting up the data portal and webpage.

References

A, G., I. Velicogna, J. S. Kimball, and Y. Kim (2015), Impact of changes in GRACE derived terrestrial water storage on vegetation growth in Eurasia, Environ. Res. Lett., 10(12), 12,4024–12,4024.

Anav, A., P. Friedlingstein, M. Kidston, L. Bopp, P. Ciais, P. Cox, C. Jones, M. Jung, R. Myneni, and Z. Zhu (2013), Evaluating the land and ocean components of the global carbon cycle in the CMIP5 Earth System Models, J. Clim., 26(18), 6801–6843.

Baldocchi, D., et al. (2001), FLUXNET: A new tool to study the temporal and spatial variability of ecosystem-scale carbon dioxide, water vapor, and energy flux densities, Bull. Am. Meteorol. Soc., 82(11), 2415–2434.

Baldocchi, D. D., L. Xu, and N. Kiang (2004), How plant functional-type, weather, seasonal drought, and soil physical properties alter water and energy fluxes of an oak-grass savanna and an annual grassland, Agric. For. Meteorol., 123, 13–39.

Baldocchi, D. D., S. Ma, S. Rambal, L. Misson, J.-M. Ourcival, J.-M. Limousin, J. Pereira, and D. Papale (2010), On the differential advantages of evergreenness and deciduousness in Mediterranean oak woodlands: A flux perspective, Ecol. Appl., 20(6), 1583–1597.

Barbeta, A., M. Mejia-Chang, R. Ogaya, J. Voltas, T. E. Dawson, and J. Penuelas (2015), The combined effects of a long-term experimental drought and an extreme drought on the use of plant-water sources in a Mediterranean forest, Global Change Biol., 21(3), 1213–1225.
Beer, C., et al. (2010), Terrestrial gross carbon dioxide uptake: Global distribution and covariation with climate, Science, 329(5993), 834–838.
Bierkens, M. F. P., et al. (2015), Hyper-resolution global hydrological modelling: What is next?, Hydrol. Processes, 29(2), 310–320.
Bonan, G. B., K. W. Oleson, R. A. Fisher, G. Lasslop, and M. Reichstein (2012), Reconciling leaf physiological traits and canopy flux data: Use of the TRY and FLUXNET databases in the Community Land Model version 4, J. Geophys. Res., 117, G02026, doi:10.1029/2011JG001913.
Breiman, L. (2001), Random forests, Mach. Learn., 45(1), 5–32.
Cohen, D., et al. (2006), Groundwater-supported evapotranspiration within glaciated watersheds under conditions of climate change, J. Hydrol., 230, 484–500.
Cramer, V. A., P. J. Thorburn, and G. W. Fraser (1999), Transpiration and groundwater uptake from farm forest plots of Casuarina glauca and Eucalyptus camaldulensis in saline areas of southeast Queensland, Australia, Agric. Water Manage., 39(2–3), 187–204.
de Graaf, I. E. M., E. H. Sutanudjaja, L. P. H. van Beek, and M. F. P. Bierkens (2015), A high resolution global scale groundwater model, Hydrol. Earth Syst. Sci., 11(5), 5217–5250.
Defries, R. S., M. C. Hansen, J. R. G. Townshend, A. C. Janetos, and T. R. Loveland (2000), A new global 1-km dataset of percentage tree cover derived from remote sensing, Global Change Biol., 6(2), 247–254.
Dirmeyer, P. A., X. Gao, M. Zhao, G. Zhichang, T. Oki, and N. Hanasaki (2006), GSWP-2: Multimodel analysis and implications for our perception of the land surface, Bull. Am. Meteorol. Soc., 87(10), 1391–1397.
Doody, T. M., O. V. Barron, K. Dowsley, I. Emelyanova, J. Fawcett, I. C. Overton, J. L. Pritchard, A. I. J. M. V. Dijk, and G. Warren (2017), Continental mapping of groundwater dependent ecosystems: A methodological framework to integrate diverse data and expert opinion, J. Hydrol.: Reg. Stud., 10, 61–81.
Eamus, D., S. Zolfaghar, R. Villalobos-Vega, J. Cleverly, and A. Huete (2015), Groundwater-dependent ecosystems: Recent insights from satellite and field-based studies, Hydrol. Earth Syst. Sci., 19(10), 4229–4256.
Fan, Y. (2015), Groundwater in the Earth's critical zone: Relevance to large-scale patterns and processes, Water Resour. Res., doi:10.1002/2015WR017037.
Fan, Y., H. Li, and G. Miguez-Macho (2013), Global patterns of groundwater table depth, Science, 339(6122), 940–943.
FLUXCOM (2017), FLUXCOM Global Energy and Carbon Fluxes, Max Planck Institute for Biogeochemistry, Jena, Germany. [Available at http://www.fluxcom.org/.]
Forkel, M., N. Carvalhais, S. Schaphoff, W. V. Bloh, M. Migliavacca, M. Thurner, and K. Thonicke (2014), Identifying environmental controls on vegetation greenness phenology through model-data integration, Biogeosciences, 11(23), 7025–7050.
Frankenberg, C., J. Berry, L. Guanter, and J. Joiner (2013), Remote sensing of terrestrial chlorophyll fluorescence from space, SPIE Newsroom, 19.
Gou, S., S. Gonzales, and G. R. Miller (2015), Mapping potential groundwater-dependent ecosystems for sustainable management, Groundwater, 53(1), 99–110.
Grimaldi, S., F. Orellana, and E. Daly (2015), Modelling the effects of soil type and root distribution on shallow groundwater resources, Hydrol. Processes, 29, 4457–4469.
Hansen, M. C., et al. (2013), High-resolution global maps of 21st-century forest cover change, Science, 342(6160), 850–853.
Hamonized World Soil Database (2008), FAO/IIASA/ISRIC/ISSCAS/JRC, Harmonized World Soil Database (version 1.0).
Ichii, K., et al. (2017), New data-driven estimation of terrestrial CO_2 fluxes in Asia using a standardized database of eddy covariance measurements, remote sensing data, and support vector regression, J. Geophys. Res. Biogeosci., doi:10.1002/2016JG003640.
Joyce, R. J., J. E. Janowiak, P. A. Arkin, and P. Xie (2004), CMORPH: A method that produces global precipitation estimates from passive microwave and infrared data at high spatial and temporal resolution, J. Hydrometeorol., 5(3), 487–503.
Jung, M., and J. Zscheischler (2013), A guided hybrid genetic algorithm for feature selection with expensive cost functions, Proc. Comput. Sci., 18, 2337–2346.
Jung, M., K. Henkel, M. Herold, and G. Churkina (2006), Exploiting synergies of global land cover products for carbon cycle modeling, Remote Sens. Environ., 101(4), 534–553.
Jung, M., et al. (2011), Global patterns of land-atmosphere fluxes of carbon dioxide, latent heat, and sensible heat derived from eddy covariance, satellite, and meteorological observations, J. Geophys. Res., 116, G00J07, doi:10.1029/2010JG001566.
Jung, M., et al. (2017), Compensatory water effects link yearly global land CO_2 sink changes to temperature, Nature, 541(7638), 516–520.
Kath, J., K. Reardon-Smith, A. F. L. Brocque, F. J. Dyer, E. Dafny, L. Fritz, and M. Batterham (2014), Groundwater decline and tree change in floodplain landscapes: Identifying non-linear threshold responses in canopy condition, Global Ecol. Conserv., 2, 148–160.
Keenan, T. F., D. Y. Hollinger, G. Bohrer, D. Dragoni, J. W. Munger, H. P. Schmid, and A. D. Richardson (2013), Increase in forest water-use efficiency as atmospheric carbon dioxide concentrations rise, Nature, 499(7458), 324–327.
Koirala, S., P. J. F. Yeh, Y. Hirabayashi, S. Kanae, and T. Oki (2014), Global-scale land surface hydrologic modeling with the representation of water table dynamics, J. Geophys. Res. Atmos., 119, 75–89, doi:10.1002/2013JD020398.
Kottek, M., J. Grieser, C. Beck, B. Rudolf, and F. Rubel (2006), World map of the Köppen-Geiger climate classification updated, Meteorol. Z., 15(3), 259–263.
Lasslop, G., M. Reichstein, D. Papale, A. D. Richardson, A. Arneth, A. Barr, P. Stoy, and G. Wohlfahrt (2010), Separation of net ecosystem exchange into assimilation and respiration using a light response curve approach: Critical issues and global evaluation, Global Change Biol., 16(1), 187–208.
Lautz, L. K. (2008), Estimating groundwater evapotranspiration rates using diurnal water-table fluctuations in a semi-arid riparian zone, Hydrogeol. J., 16(3), 483–497.
Lehner, B., K. Verdin, and A. Jarvis (2008), New global hydrography derived from spaceborne elevation data, Eos Trans. AGU, 89(10), 93–94.
Martinet, M. C., E. R. Vivoni, J. R. Cleverly, J. R. Thibault, J. F. Schuetz, and C. N. Dahm (2009), On groundwater fluctuations, evapotranspiration, and understory removal in riparian corridors, Water Resour. Res., 45, W05425, doi:10.1029/2008WR007152.
Maxwell, R. M., and L. E. Condon (2016), Connections between groundwater flow and transpiration partitioning, Science, 353(6297), 377–380.
McGrath, G. S., R. Sadler, K. Fleming, P. Tregoning, C. Hinz, and E. J. Veneklaas (2012), Tropical cyclones and the ecohydrology of Australia's recent continental-scale drought, Geophys. Res. Lett., 39, L03404, doi:10.1029/2011GL050263.
Moderate Resolution Imaging Spectroradiometer (2012), NASA Land Processes Distributed Active Archive Center (LP DAAC): The Moderate Resolution Imaging Spectroradiometer (MODIS) data, USGS/Earth Resources Observation and Science (EROS) Center, Sioux Falls, South Dakota.
Moreno-Casasola, P., and G. Vázquez (1999), The relationship between vegetation dynamics and water table in tropical dune slacks, J. Veg. Sci., 515–524.

Naumburg, E., R. Mata-gonzalez, R. Hunter, T. McLendon, and D. Martin (2005), Phreatophytic vegetation and groundwater fluctuations: A review of current research and application of ecosystem response modeling with an emphasis on Great Basin vegetation, Environ. Manage., 35(6), 726–740.

Neill, C., et al. (2013), Watershed responses to Amazon soya bean cropland expansion and intensification, Philos. Trans. R. Soc. London, Ser. B, 368(1619), doi:10.1098/rstb.2012.0425.

Niu, G. Y., Z. L. Yang, R. E. Dickinson, L. E. Gulden, and H. Su (2007), Development of a simple groundwater model for use in climate models and evaluation with Gravity Recovery and Climate Experiment data, J. Geophys. Res., 112, D07103, doi:10.1029/2006JD007522.

NOAA (2011), NOAA CPC Morphing Technique (CMORPH) global precipitation analyses, Climate Prediction Center/National Centers for Environmental Prediction/National Weather Service/NOAA/U.S. Dep. of Commerce, Accessed 15 April 2014.

Orellana, F., P. Verma, S. P. Loheide, and E. Daly (2012), Monitoring and modeling water-vegetation interactions in groundwater-dependent ecosystems, Rev. Geophys., 50, RG3003, doi:10.1029/2011RG000383.

Parolin, P., and F. Wittmann (2010), Struggle in the flood: Tree responses to flooding stress in four tropical floodplain systems, AoB Plants, 2010, plq003-plq003.

Pérez Hoyos, I. C., N. Y. Krakauer, R. Khanbilvardi, and R. A. Armstrong (2016), A review of advances in the identification and characterization of groundwater dependent ecosystems using geospatial technologies, Geosciences, 6(2), 17, doi:10.3390/geosciences6020017.

Piao, S., et al. (2013), Evaluation of terrestrial carbon cycle models for their response to climate variability and to CO_2 trends, Global Change Biol., 19(7), 2117–2132.

Reichstein, M., et al. (2005), On the separation of net ecosystem exchange into assimilation and ecosystem respiration: Review and improved algorithm, Global Change Biol., 11(9), 1424–1439.

Richey, A. S., B. F. Thomas, M.-H. Lo, J. T. Reager, J. S. Famiglietti, K. Voss, S. Swenson, and M. Rodell (2015), Quantifying renewable groundwater stress with GRACE, Water Resour. Res., 51, 5217–5238, doi:10.1002/2015WR017349.

Rodriguez-Iturbe, I., P. D'Odorico, F. Laio, L. Ridolfi, and S. Tamea (2007), Challenges in humid land ecohydrology: Interactions of water table and unsaturated zone with climate, soil, and vegetation, Water Resour. Res., 43, W09301, doi:10.1029/2007WR006073.

Silvertown, J., Y. Araya, and D. Gowing (2015), Hydrological niches in terrestrial plant communities: A review, J. Ecol., 103(1), 93–108.

Still, C. J., J. A. Berry, G. J. Collatz, and R. S. DeFries (2003), Global distribution of C3 and C4 vegetation: Carbon cycle implications, Global Biogeochem. Cycles, 17(1), 1006, doi:10.1029/2001GB001807.

Tramontana, G., K. Ichii, G. Camps-Valls, E. Tomelleri, and D. Papale (2015), Uncertainty analysis of gross primary production upscaling using random forests, remote sensing and eddy covariance data, Remote Sens. Environ., 168, 360–373.

Tramontana, G., et al. (2016), Predicting carbon dioxide and energy fluxes across global FLUXNET sites with regression algorithms, Biogeosciences, 13(14), 4291–4313.

Tron, S., F. Laio, and L. Ridolfi (2014), Effect of water table fluctuations on phreatophytic root distribution, J. Theor. Biol., 360, 102–108.

USGS (1996), Global 30-arc-second elevation data set, U.S. Geol. Surv. Sioux Falls, South Dakota.

Weltzin, J. F., and G. R. McPherson (1997), Spatial and temporal soil moisture resource partitioning by trees and grasses in a temperate savanna, Arizona, USA, Oecologia, 112(2), 156–164.

Yang, F., K. Ichii, M. A. White, H. Hashimoto, A. R. Michaelis, P. Votava, A. X. Zhu, A. Huete, S. W. Running, and R. R. Nemani (2007), Developing a continental-scale measure of gross primary production by combining MODIS and AmeriFlux data through support vector machine approach, Remote Sens. Environ., 110(1), 109–122.

Yang, Y., D. Long, H. Guan, B. R. Scanlon, C. T. Simmons, L. Jiang, and X. Xu (2014), GRACE satellite observed hydrological controls on interannual and seasonal variability in surface greenness over mainland Australia, J. Geophys. Res. Biogeosci., 119, 2245–2260, doi:10.1002/2014JG002670.

Yeh, P. J. F., and J. S. Famiglietti (2009), Regional groundwater evapotranspiration in Illinois, J. Hydrometeorol., 10, 464–478.